CHEMISTRY
A EUROPEAN JOURNAL

DOI: 10.1002/chem.201001087

Enantiomerically Pure Alleno–Acetylenic Macrocycles: Synthesis, Solid-State Structures, Chiroptical Properties, and Electron Localization Function Analysis

Pablo Rivera-Fuentes,[a] José Lorenzo Alonso-Gómez,[b] Ana G. Petrovic,[b] Paul Seiler,[a] Fabrizio Santoro,[c] Nobuyuki Harada,[b] Nina Berova,[b] Henry S. Rzepa,*[d] and François Diederich*[a]

Dedicated to Professor José Barluenga on the occasion of his 70th birthday

Abstract: New enantiomerically pure alleno–acetylenic macrocycles were prepared by oxidative homocoupling of optically active 1,3-diethynylallenes. Enantiomer separation resulted from a combined strategy of synthesis and chiral HPLC techniques. Two other achiral stereoisomers were also isolated and fully characterized. In addition, the X-ray structures of the chiral D_4- and C_2-symmetric macrocycles are reported. The chiroptical properties of these macrocycles are discussed on the basis of quantum chemical calculations, by using the CAM-B3LYP functional. Studies were carried out to investigate the vibronic fine structure observed experimentally in the UV/Vis and CD spectra. The origin of the intense chiroptical response of the chiral alleno–acetylenic macrocycles is explained by considering the topology of the molecular orbitals involved, thus relating electronic properties to structural features. Further analysis of the canonical molecular orbitals and the electron localization function (ELF) shows that these macrocycles belong to a relatively rare class of highly stable and formally anti-aromatic Hückel compounds.

Keywords: allenes · aromaticity · chirality · circular dichroism · macrocycles

Introduction

Acetylenic shape-persistent macrocycles are among the most interesting structures in modern organic chemistry. These carbon-rich systems have been used in a very broad range of applications, including formation of liquid-crystalline phases,[1] extended tubular channels in solution,[2] porous organic solids,[3] aggregates on surfaces,[4] and host–guest complexes.[5] Furthermore, the properties of these macrocycles have also been extensively studied. Particularly interesting features include their second- and third-order nonlinear optical behavior,[6] and their electrochemical[7] and chiroptical properties.[8,9] In addition, they have been exploited by theoreticians to gain insight into the intriguing electronic properties of acetylenic structures.[10]

Most shape-persistent macrocycles are based on arylacetylenic building blocks. A variety of methods and strategies for the construction of phenylacetylene-[11] and other arylacetylene-based[12] macrocycles have been published. However, advantages of macrocycles containing conjugated all-carbon backbones without annellated aryl units have been pointed out recently.[13] Such compounds have mostly been prepared as potential molecular precursors of still elusive, two-dimensional (2D) carbon networks, and some examples include perethynylated dehydroannulenes, expanded radialenes, and radiaannulenes.[13,14] While 2D acetylenic scaffolding has been vigorously pursued, three-dimensional (3D)

[a] P. Rivera-Fuentes, P. Seiler, Prof. F. Diederich
Laboratorium für Organische Chemie, ETH Zürich
Hönggerberg, HCI, 8093 Zürich (Switzerland)
Fax: (+41) 44-632-1109
E-mail: diederich@org.chem.ethz.ch

[b] Dr. J. L. Alonso-Gómez, Dr. A. G. Petrovic, Prof. N. Harada, Prof. N. Berova
Department of Chemistry, Columbia University
10027 New York (USA)

[c] Dr. F. Santoro
Istituto per i Processi Chimico-Fisici-CNR
Area della Ricerca del CNR, Via Moruzzi, 1 I-56124 Pisa (Italy)

[d] Prof. H. S. Rzepa
Department of Chemistry, Imperial College London
South Kensington Campus, Exhibition Road
London, SW7 2AY (UK)

Supporting information for this article is available on the WWW under http://dx.doi.org/10.1002/chem.201001087.

acetylenic scaffolding with all-carbon backbones without aryl spacers remains limited to very few examples, namely a buta-1,3-diyne-1,4-diyl-expanded cubane[15] and alleno–acetylenic macrocycles and foldamers[9,16–18]

Shape-persistent alleno–acetylenic macrocycles with inherent chirality are of interest from many points of view. Their conformational rigidity and asymmetry can be used to relate chiroptical properties to structural features. In addition, functionalization of the exocyclic allenic substituents promises new approaches to build up chiral supramolecular assemblies in solution and in the solid state. Asymmetric alleno–acetylenic macrocycles could also be used to induce macroscopic chirality, leading to optically active liquid-crystalline phases in solution or to chiral patterns on surfaces. Molecular recognition in their chiral cavities also remains to be explored.

From the theoretical point of view, allene-containing macrocycles are also of great interest. Allenes have been predicted to impart half-turns to π-electronic manifolds to furnish Möbius and Hückel aromatic and anti-aromatic compounds.[19] It has been proposed that chiroptical properties, such as electronic circular dichroism (CD) and optical rotatory dispersion (ORD), could be crucial in the experimental characterization of novel chiral aromaticities.[20] In this regard, enantiopure, shape-persistent, alleno–acetylenic macrocycles provide a unique opportunity to find chiroptical "fingerprints" of chiral π-electronic manifolds.

Recently, we reported the enantioselective synthesis and optical resolution of stable, optically pure 1,3-diethynylallenes (DEAs) bearing *tert*-butyl moieties to protect the allene moiety.[21] Alleno–acetylenic macrocycles obtained from these DEA building blocks show high thermal, chemical, and photochemical stability.[9,17] Herein, we report the synthesis of two enantiomeric alleno–acetylenic macrocycles and their two achiral stereoisomers, taking a different approach from the one reported in an earlier communication.[9] The solid-state structures of two chiral macrocycles were solved, providing unambiguous configurational assignments. Chiroptical properties are analyzed on the basis of time-dependent quantum chemical calculations, and comments about the vibronic fine structure observed in the UV/Vis and CD spectra are provided. Based on these calculations, an explanation of the origin of the remarkably intense chiroptical response in the chiral alleno–acetylenic macrocycles is proposed. Finally, analysis of canonical molecular orbitals (MOs) and the electron localization function (ELF) delivers conclusions about the extent of aromaticity of these systems.

Results and Discussion

Synthesis: In a previous communication,[9] we hypothesized that macrocyclization of a racemic DEA building block by acetylenic homocoupling, following the three-step protocol shown in Scheme 1, would lead to six stereoisomers of macrocycle **1**. The DEA derivative **2** was dimerized by Pd-catalyzed oxidative homocoupling,[22] using air as oxidant and *N*,*N*,*N*′,*N*′-tetramethylethylenediamine (TMEDA) as base to obtain **3** quantitatively. Deprotection to deliver dimer **4** was performed in good yield by treatment with NaOH in toluene at 90 °C. Macrocycle **1** was obtained in a one-pot dimerization-cyclization reaction of compound **4** under Eglinton–Galbraith conditions.

The expected stereoisomers of **1** are two racemates and two achiral diastereoisomers. The D_4-symmetric (all the *tert*-butyl groups are magnetically equivalent) enantiomers (*M*,*M*,*M*,*M*)-(+)-**1** and (*P*,*P*,*P*,*P*)-(−)-**1**, with crown geometry, were prepared and characterized earlier using the enantiomerically pure DEAs (*M*)-(−)-**2** and (*P*)-(+)-**2**, respectively.[9] The other racemate is the C_2-symmetric (four magnetically different *tert*-butyl groups) (*M*,*M*,*M*,*P*)/(*P*,*P*,*P*,*M*)-**1** pair with twist geometry. The two achiral isomers are C_{2h}-symmetric (two magnetically different *tert*-butyl groups) (*P*,*P*,*M*,*M*)-**1** with chair geometry and D_{2d}-symmetric (all the *tert*-butyl groups are magnetically equivalent) (*P*,*M*,*P*,*M*)-**1** with boat geometry (Figure 1).

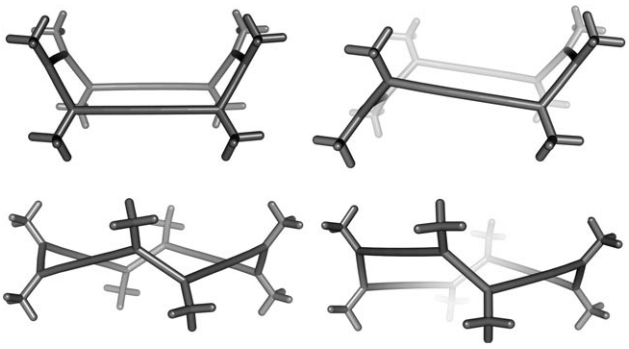

Figure 1. Isomers of **1**. From top left to bottom right: ((*P*,*M*,*P*,*M*)-**1** boat), ((*P*,*P*,*M*,*M*)-**1** chair), ((*P*,*P*,*P*,*P*)-(−)-**1** crown), and ((*P*,*P*,*P*,*M*)-(−)-**1** twist). Hydrogen atoms are not shown.

In order to prove that all isomers are actually formed, the synthesis depicted in Scheme 1 was performed using (±)-**2**. The macrocyclization afforded a white solid that displayed a ^{1}H NMR spectrum with five partially overlapped signals between 1.153 and 1.167 ppm (Figure 2, lowest spectrum). The absence of signals corresponding to terminal acetylenic hydrogen atoms confirmed the cyclic nature of the products. Gel permeation chromatographic analysis ruled out the presence of larger macrocycles. Separation of the mixture by using recycling HPLC delivered four compounds in a 1:4:2:1 ratio (in order of elution, for details see the Experimental Section). The first compound eluted had a ^{1}H NMR spectrum with one singlet at 1.157 ppm, the second compound eluted showed four singlets at 1.153, 1.157, 1.161, and 1.162 ppm, the third compound showed two singlets at 1.153 and 1.168 ppm, and the fourth compound showed a singlet at 1.161 ppm (Figure 2). The fourth compound eluted had identical ^{1}H and ^{13}C NMR spectra to those of the previously obtained (*M*,*M*,*M*,*M*)-(+)-**1** and (*P*,*P*,*P*,*P*)-(−)-**1**, and there-

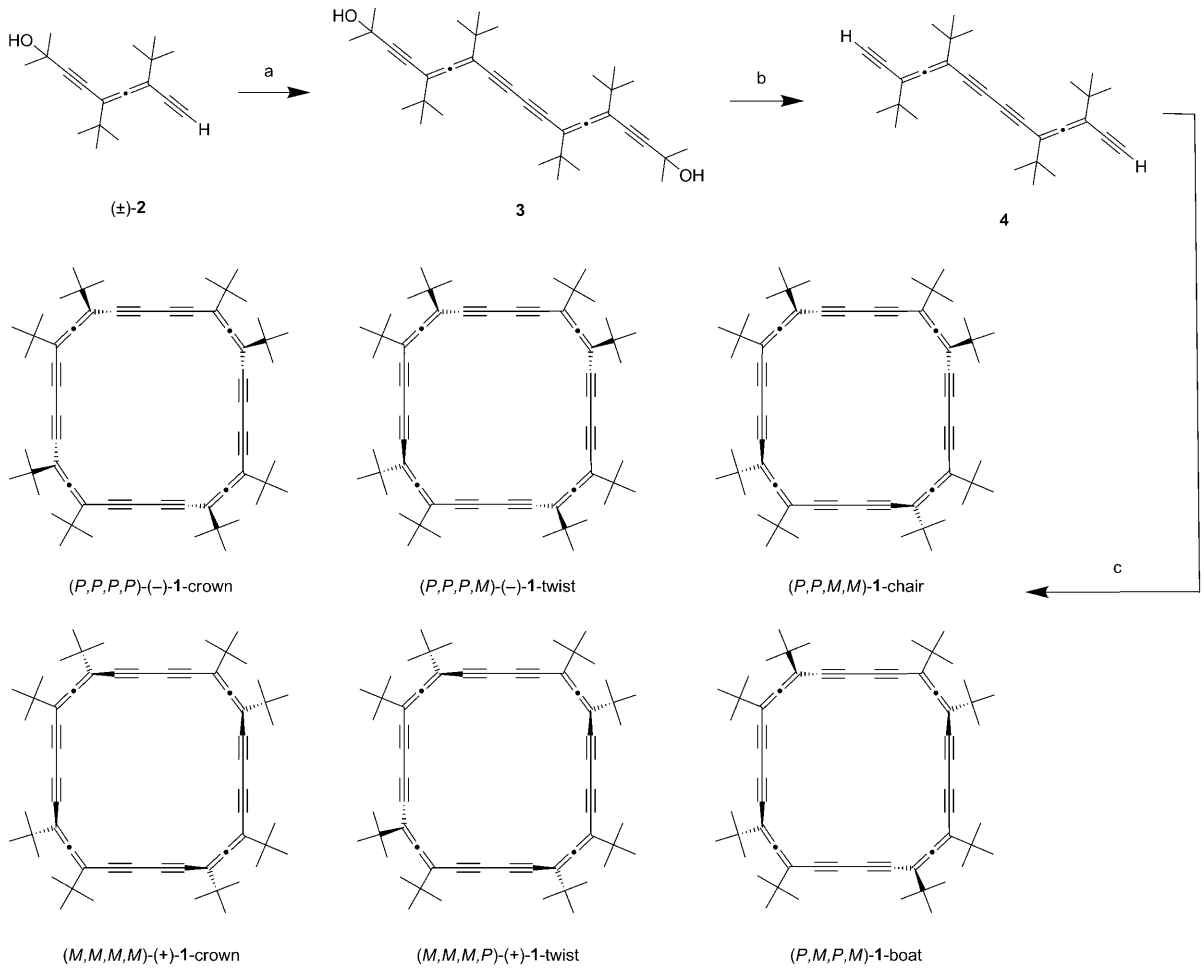

Scheme 1. Synthesis of macrocycles **1**. Reagents and conditions: a) $[PdCl_2(PPh_3)_2]$, CuI, TMEDA, air, toluene, 50 °C, 24 h, 99 %; b) NaOH, toluene, 90 °C, 10 h, 65 %; c) CuCl, $CuCl_2$, pyridine, 20 °C, then addition of **4** as a mixture of stereoisomers over 20 h, 70 %. TMEDA = *N*,*N*,*N*′,*N*′-tetramethylethylenediamine.

fore was assigned to be the (*M*,*M*,*M*,*M*)/(*P*,*P*,*P*,*P*)-**1** crown racemate. Based on symmetry considerations, the first compound eluted was assigned to the (*P*,*M*,*P*,*M*)-**1** boat isomer, the second compound eluted to the (*M*,*M*,*M*,*P*)/(*P*,*P*,*P*,*M*)-**1** twist racemate, and the third compound eluted to the (*P*,*P*,*M*,*M*)-**1** chair isomer. The isomeric ratio corresponds to the statistically expected one, demonstrating that there is no preference for the formation of a particular stereoisomer.

Taking advantage of the statistical distribution of isomers, a strategy was envisioned for the synthesis of the enantiomerically enriched twist isomer. When the synthesis depicted in Scheme 1 is performed using a mixture of (*P*)-(+)-**2**/(*M*)-(−)-**2** 91:9 as starting material, the macrocycles should be obtained in the ratio shown in Table 1.

According to this ratio, after separation of the diastereoisomers, the crown and twist isomers should be isolable in an enantiomeric ratio (e.r.) of (*P*,*P*,*P*,*P*)-(−)-**1**/(*M*,*M*,*M*,*M*)-(+)-**1** > 99:1, and (*P*,*P*,*P*,*M*)-(−)-**1**/(*M*,*M*,*M*,*P*)-(+)-**1** ≈ 99:1, respectively.

The synthesis shown in Scheme 1 was subsequently performed with a mixture (*P*)-(+)-**2**/(*M*)-(−)-**2** 91:9 (determined by HPLC), and the products of the last step were separated by recycling HPLC. The chromatogram showed traces of the boat and chair isomers, and a relation of crown/twist isomers of approximately 2:1, in agreement with the statistically predicted ratio (Table 1). The chiroptical properties of the (*P*,*P*,*P*,*P*)-(+)-**1** crown isomer isolated by this method were identical to those previously reported for enantiopure material.[9] All these facts confirmed that the twist isomer (*P*,*P*,*P*,*M*)-(−)-**1** was obtained in very high enantiomeric ratio (≈99:1). The synthesis of the (*M*,*M*,*M*,*P*)-(+)-**1** enantiomer was performed in the same way. Full spectroscopic characterization of all stereoisomers is provided in the Experimental Section, and ^{13}C NMR spectra can be found in the Supporting Information.

Solid-state structures: The structures of racemates (*P*,*P*,*P*,*P*)/(*M*,*M*,*M*,*M*)-**1** and (*P*,*P*,*P*,*M*)/(*M*,*M*,*M*,*P*)-**1** were further confirmed by X-ray diffraction studies. Single crystals of the (*P*,*P*,*P*,*P*)/(*M*,*M*,*M*,*M*)-**1** racemate, suitable for X-ray analysis, were obtained by slow evaporation of a mixture of hexane/ethanol/methanol 9:0.5:0.5. The investigated crystal

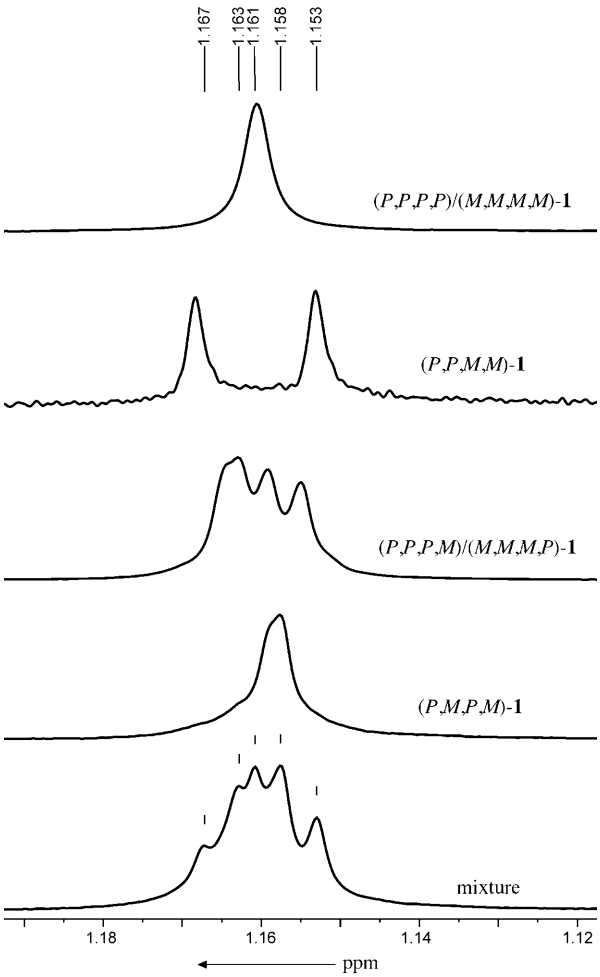

Figure 2. Stacking of ^{1}H NMR (300 MHz, $CDCl_3$) spectra of the mixture of stereoisomers of **1** and the individual spectra (arbitrary intensities) after recycling HPLC separation.

(highly solvated and extremely fragile) was mounted at low temperature to prevent evaporation of enclosed solvents. The crystal was found to be tetragonal, space group *P*4/*nnc* (for further details, see the Experimental Section).

Two conformers of (*P*,*P*,*P*,*P*)/(*M*,*M*,*M*,*M*)-**1** were found in the asymmetric unit. In addition to the D_4-symmetric structure, a C_2-symmetric conformer was also found in the crystal lattice. When the latter was optimized at the B3LYP/6-31G* level of theory, it converged to the D_4-symmetric conformer. This calculation suggests that the C_2-symmetric conformer is probably a consequence of crystal packing forces. The geometry of the D_4-symmetric conformer (Figure 3) is in agreement with the structure predicted earlier by theoretical calculations,[9] and the torsion angle between neighboring allenes is around $\pm 102°$, in contrast to the torsion angle of $0 \leq \theta \leq 45$ predicted for its open chain analogue.[17]

Single crystals of the (*P*,*P*,*P*,*M*)/(*M*,*M*,*M*,*P*)-**1** racemate, suitable for X-ray analysis, were obtained by slow evaporation of a mixture of hexane/ethanol/methanol 9:0.5:0.5. This crystal was also mounted at low temperature to prevent

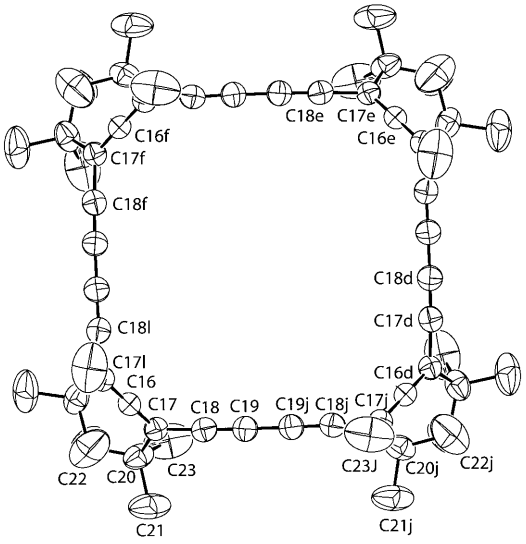

Figure 3. X-ray crystal structure of (*P*,*P*,*P*,*P*)/(*M*,*M*,*M*,*M*)-**1**. ORTEP plot of the D_4-symmetric conformer. Arbitrary numbering, atomic displacement parameters obtained at 260 K are drawn at 30% probability level (for details see the Experimental Section). Selected bond lengths [Å], bond angles [°], and torsion angles [°]: C16–C17 1.295(6), C17–C18 1.427(8), C18–C19 1.215(8), C19–C19j 1.367(8), C16f-C17f-C18f 117.0(5), C18-C17-C17l-C18l 85.6(6), C16-C17-C17j-C16d −102.5(6).

evaporation of enclosed solvents and was found to be monoclinic, space group $P2_1/n$. In this case, only one conformer (approximately C_2-symmetric, Figure 4) was found in the crystal. This conformer found in the solid state also agrees with the minimum found at the B3LYP/6-31G* level of theory.

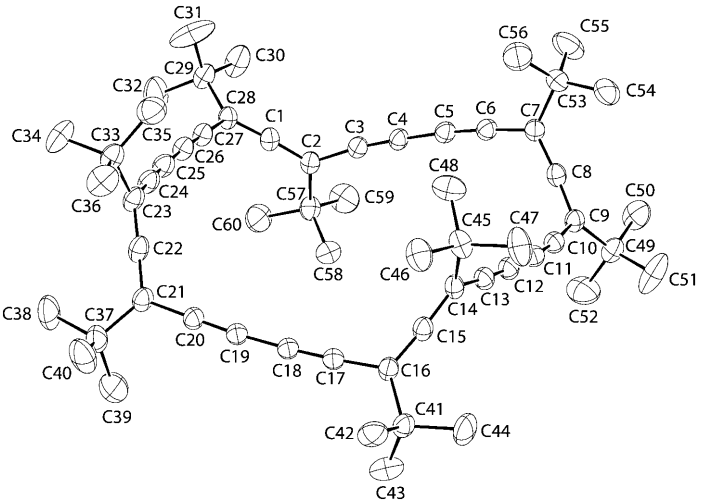

Figure 4. ORTEP plot of (*P*,*P*,*P*,*M*)/(*M*,*M*,*M*,*P*)-**1**. Arbitrary numbering, atomic displacement parameters obtained at 220 K are drawn at 30% probability level (for details see the Experimental Section). Selected bond lengths [Å], bond angles [°] and torsion angles [°]: C15–C16 1.308(5), C16–C17 1.436(6), C17–C18 1.203(7), C18–C19 1.383(7), C20-C21-C22 119.5(4), C8-C9-C10 116.8(3), C1-C2-C7-C8 119.8(4), C8-C9-C14-C15 135.9(4), C15-C16-C21-C22 −37.6(4), C22-C23-C28-C1 −4.1(4).

Table 1. Statistical distribution of stereoisomers [%] of macrocycle **1**, starting from optically enriched DEA **2**.

(*P*)-(+)-**2**				(*M*)-(−)-**2**	
91				9	
(*P,P*)-(+)-**4**		(*P,M*)-**4**		(*M,M*)-(−)-**4**	
82.8		16.4		0.8	
(*P,P,P,P*)-(−)-**1** Crown	(*P,P,P,M*)-(−)-**1** Twist	(*P,M,P,M*)-**1** Boat	(*P,P,M,M*)-**1** Chair	(*M,M,M,P*)-(+)-**1** Twist	(*M,M,M,M*)-(+)-**1** Crown
68.6	27.2	1.3	2.6	0.3	<0.01

Chiroptical properties: In the earlier communication, we reported the unusually intense CD of enantiomers (*P,P,P,P*)-(−)-**1** and (*M,M,M,M*)-(+)-**1**.[9] Cotton effects of enantiomers (*P,P,P,M*)-(−)-**1** and (*M,M,M,P*)-(+)-**1** are less intense and their CD profiles are different. These divergences can be attributed to the dissimilar symmetries of the molecules, in particular because of the different torsion angles between neighboring allenes (102° in (*M,M,M,M*)-**1** and 120, 136, −38, and −4° in (*M,M,M,P*)-**1**). UV/Vis and CD spectra of both pairs of enantiomers are shown in Figure 5.

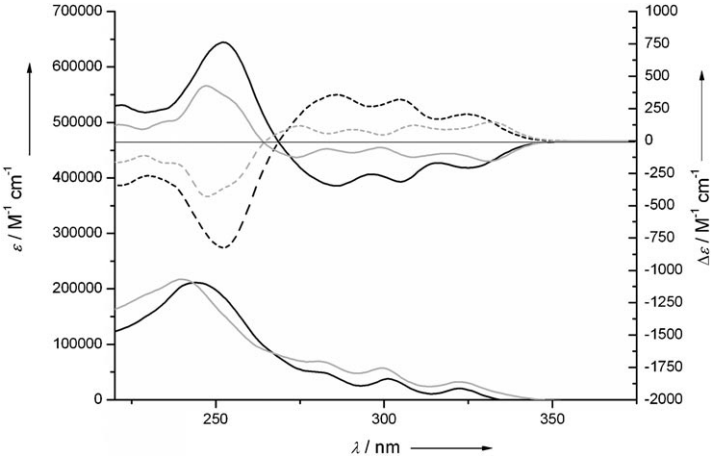

Figure 5. CD spectra (upper chart) of (*M,M,M,M*)-(+)-**1** (dashed black line), (*P,P,P,P*)-(−)-**1** (solid black line), (*M,M,M,P*)-(+)-**1** (dashed grey line), and (*P,P,P,M*)-(−)-**1** (solid grey line) measured in *n*-hexane. UV/Vis spectra (lower chart) of (*P,P,P,P*)-(−)-**1** (black line) and (*P,P,P,M*)-(−)-**1** (grey line).

Through our previous investigations of enantiopure DEA oligomers[17] and macrocycles[9] (*M,M,M,M*)-(+)-**1** and (*P,P,P,P*)-(−)-**1**, we established that these molecules exhibit exceptional chiroptical responses manifested through unprecedented CD intensities. In the case of DEA oligomers, the nonlinear enhancement of CD and ORD from dimer to octamer/hexadecamer has been related to a conformational preference along the backbone. Correlation between experimental spectra and quantum mechanical predictions of CD and ORD responses enabled us to propose an ensemble of single-handed helical conformers for these oligomers. Our previous theoretical analysis[9,17] of alleno–acetylenic macromolecules was carried out at various levels of theory including the semiempirical ZINDO, time-dependent Hartree–Fock (TD-HF), and time-dependent density functional theory (TD-DFT) employing a variety of functionals and basis sets.

Although most of these methods provided similar CD profiles, we are aware of the deficiencies of the TD-DFT methodology. It has been observed that conventional functionals are unreliable for evaluating electronic properties, polarizability, and hyperpolarizability in compounds exhibiting moderate to extended π conjugation,[23] as is the case for alleno–acetylenic macromolecules. In 2004, Yanai et al.[24] introduced the Coulomb-attenuated hybrid exchange-correlation functional (CAM-B3LYP), which has the same correlation functional as the traditional B3LYP functional, but combines the exact Hartree–Fock and DFT exchange in a ratio depending on the interelectronic distance. A number of recent reports have demonstrated these improvements.[25] These studies included molecules containing oligoyne and oligoene moieties as benchmark systems due to the strong correlation between their nonlinear optical properties and their geometrical characteristics. In the present study, we employed the CAM-B3LYP functional for the investigation of the chiroptical properties of alleno–acetylenic macromolecules.

As evidenced in Figure 6, CAM-B3LYP provides a satisfactory reproduction of the main CD features for the crown macrocycle (*P,P,P,P*)-(−)-**1** with the exception of the fine structure of the negative Cotton effect. In fact, the vertical transition energies are in a notably better agreement with experimental data in comparison to data from the TD-HF and ZINDO levels of theory, which exhibit ≈1 eV over- and underestimation respectively (Figure 6). The previously assigned (*P,P,P,P*) absolute configuration of crown (−)-**1** was again confirmed by this quantum mechanical calculation of the CD spectrum. As it can be seen in Figure 6, the CD response is mainly due to the contributions of three electronic transitions: the negative Cotton effect originates from transition S1 and the positive Cotton effect from joint contributions of degenerate transitions S2 and S3. It should be noted that all methods used previously to study the chiroptical response of alleno–acetylenic structures provide the same qualitative information, and our earlier conclusions are confirmed by the CAM-B3LYP results. Although the main Cotton effect features are optimally reproduced by CAM-B3LYP, additional efforts in this study were directed to the

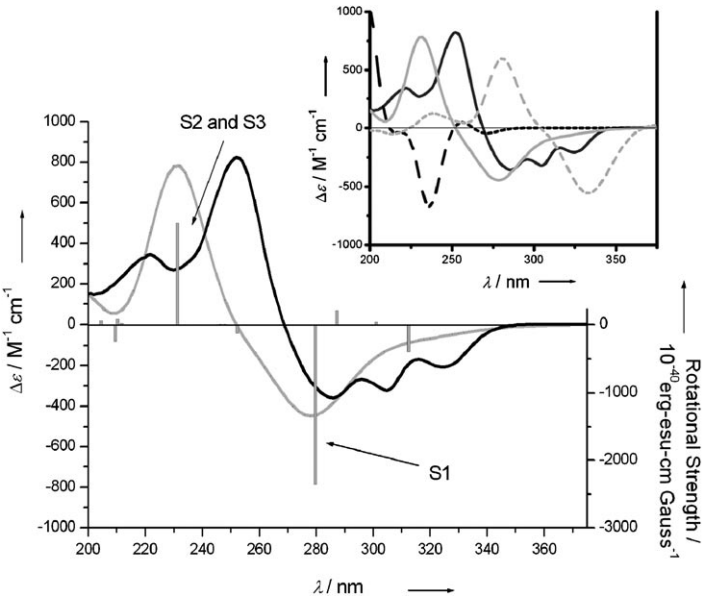

Figure 6. Experimental (black line) and simulated CD spectrum of (*P,P,P,P*)-(−)-**1** (grey line, scaled by 0.6, not shifted, rotational strength in grey bars) at the CAM-B3LYP/6-31G(d) level of theory. The inset shows experimental (black line) and simulated CD spectrum of (*P,P,P,P*)-(−)-**1** at the HF/6-31G(d) (dashed black line scaled by 0.2, not shifted), ZINDO (dashed grey line scaled by 0.4, not shifted), and CAM-B3LYP/6-31G(d) (grey line scaled by 0.6, not shifted) levels of theory.

ab initio prediction of the vibronic fine structure of transition S1.

In our previous studies on the DEA dimer **4**,[17] an analogous pattern of peaks with a regular spacing of about 2200 cm^{-1} was accurately reproduced by a full-harmonic adiabatic approach (including displacements, frequency changes, and Duschinsky mixings)[26a] and assigned to a progression along the symmetric combination of the CC triple-bond stretching. In the D_4-symmetric (*P,P,P,P*)-(−)-**1**, the eight CC triple-bond stretchings are combined in eight collective normal modes (two degenerate pairs of *E* symmetry, plus four modes belonging to the A_2, A_1, B_1 and B_2 irreducible representations, respectively). Their harmonic frequencies, according to CAM-B3LYP/6-31G(d) calculations, span a narrow frequency region from 2300 to 2400 cm^{-1}, showing that these modes are separated from the lower frequency modes by more than 200 cm^{-1}, and from the higher frequency ones by more than 600 cm^{-1}. Considering that the computed frequencies are usually overestimated by a factor of $\approx 1/0.95$, it is reasonable to assign that the progression observed in the CD spectrum of the macrocycle (average spacing about ≈ 2200 cm^{-1}) originates from displacements along these eight modes.

The first attempt to uncover the origin of the observed vibrational structure was to use the adiabatic model.[26] However, the dimension of the system, along with the dense manifold of electronic states around transition S1, precludes optimization of the excited state geometry, which is a prerequisite for applying the adiabatic model.[26c] Therefore, it was not possible to simulate the CD line shape with the single-state adiabatic approach adopted for the DEA dimer **4**.[26a]

Trying to overcome this challenge, we used a simplified model to compute the spectrum, namely the vertical gradient (VG) approach, in which normal modes and frequencies of the excited state are assumed to be equal to those of the ground state. Although this alternative model only accounts for the effect of total symmetric a_1 modes, it reproduces the full-harmonic results obtained for the dimeric alleno–acetylenic structure **4** previously reported.[17]

However, application of the VG method in (*P,P,P,P*)-(−)-**1** did not provide a satisfactory prediction of the experimental vibrational fine structure. A progression along the a_1 collective CC triple bond stretching is actually predicted, but it is strongly underestimated. However, we are aware of the fact that due to the symmetry of the molecule and the dense manifold of states, Jahn–Teller and pseudo Jahn–Teller effects might be operative. Therefore, more refined theoretical modelling including non-adiabatic effects would be needed for a simulation of the spectrum which is beyond the current state-of-the-art methods.

Origin of CD spectra based on MO analysis: As shown in Figure 6, the CD spectrum of (*P,P,P,P*)-(−)-**1** shows extraordinary strong Cotton effects. This fact indicates that the rotational strength, which is proportional to the product of electric transition dipole moment (ETDM) and magnetic transition dipole moment (MTDM), is very large. To gain insight into the mechanism of such outstanding Cotton effects of (*P,P,P,P*)-(−)-**1**, the origin of the ETDM and MTDM for each relevant electronic transition was studied on the basis of the topology of the MOs involved.

As mentioned before, the CD response of the (*P,P,P,P*)-(−)-**1** macrocycle mainly arises from transition S1 and degenerate transitions S2 and S3 (Figure 6). The calculated ETDM and MTDM of the transition S1 are depicted in Figure 7a, in which both transition moments are parallel to the *z* axis (C_4-symmetry axis). Namely the MTDM is parallel to the *z* axis, while the ETDM is anti-parallel to the *z* axis, and therefore, the rotational strength is negative yielding a negative Cotton effect. The characteristic of transition S1 is that its MTDM is extraordinarily large, which consequently contributes to the intense Cotton effects. On the other hand, the ETDM of transition S1 is very small, which means that the transition S1 is electrically weak, but magnetically allowed and strong. Therefore, the *g*-factor ($g = \Delta\varepsilon/\varepsilon$) of the transition S1 is large, as observed experimentally.[9]

The calculated MTDM and ETDM of the transition S2 are perpendicular to the *z* axis as shown in Figure 7b. Both transition moments are in the *xy* plane, the plane intersecting all four sp carbons of the allene moieties (see Figure 7). The MTDM is thus parallel to the ETDM generating a positive Cotton effect in agreement with the observed CD. The ETDM of transition S2 is larger than that of transition S1 as shown in Figure 7, and hence the transition is electrically allowed. Since transitions S2 and S3 are degenerate, the same is true for the transition S3.

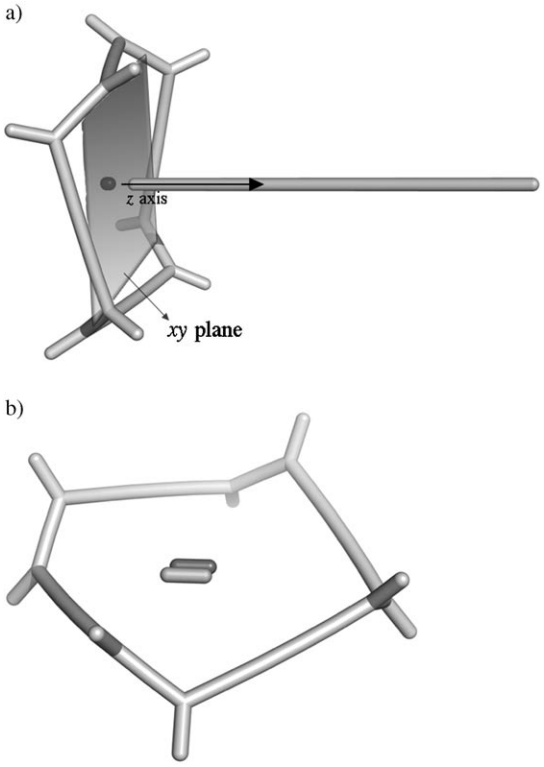

Figure 7. Schematic representation of ETDM (dark grey) and MTDM (light grey) of a) transition S1 and b) transitions S2 and S3 for the (*P*,*P*,*P*,*P*)-**1** crown macrocycle at the CAM-B3LYP/6-31G(d) level of theory. For clarity, *tert*-butyl groups were replaced by methyl groups and hydrogen atoms are not shown.

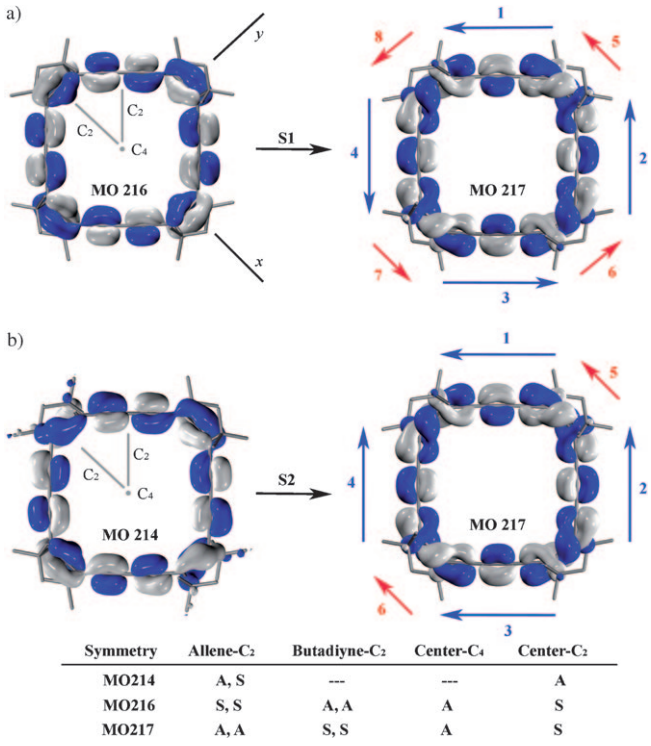

Symmetry	Allene-C_2	Butadiyne-C_2	Center-C_4	Center-C_2
MO214	A, S	---	---	A
MO216	S, S	A, A	A	S
MO217	A, A	S, S	A	S

Scheme 2. MOs and symmetry involved in the CIs of a) transition S1 and b) transition S2. In the table below, S and A indicate symmetry and antisymmetry, respectively.

The characteristic features of the MTDM and ETDM of transition S1 can be qualitatively explained by the topology and symmetry of the MOs involved in the transition. For example, one of the configuration interactions (CIs) contributing significantly to transition S1 is HOMO (MO216)→LUMO (MO217), the two MOs of which are depicted in Scheme 2a. Both MOs are mostly distributed in the *xy* plane. When looking at the butadiyne part, the transition generates the local ETDMs as indicated by the long arrows, which are arranged around the ring (Figure 8a). Therefore, the *xy* components of the local ETDMs cancel each other, while the *z* component remains non-zero, because the butadiyne units are tilted into the *z* axis. Consequently, the total ETDM has a small *z* component.

The circular arrangement of local ETDMs generates a very large MTDM, which is parallel to the *z*-axis. The MTDM is theoretically proportional to the vector product, $\vec{\mathbf{r}} \times \vec{\mu}$, in which $\vec{\mathbf{r}}$ is the distance vector from the center of ring to the local ETDM $\vec{\mu}$. The local MTDMs generated by four ETDMs arranged in a circle are perpendicular to the $\vec{\mathbf{r}}$ and $\vec{\mu}$ vectors, and hence the total MTDM of this ring system is parallel to the *z* axis and becomes very large, while the *xy* components of the local MTDMs cancel each other. The transition S1 is thus magnetically large but electrically weak as shown in Figure 7a.

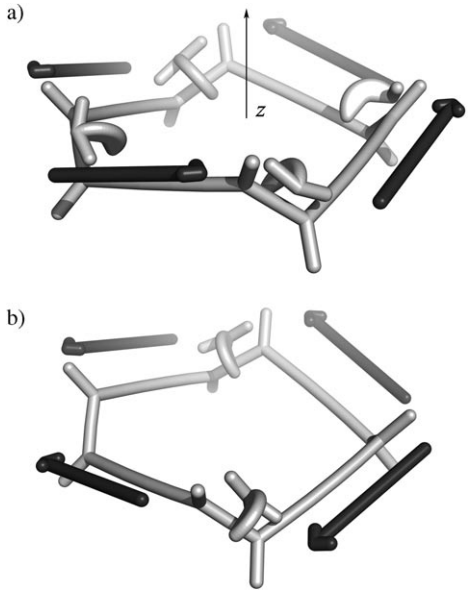

Figure 8. Schematic representation of electron motion in a) transition S1 and b) transitions S2 and S3 for the (*P*,*P*,*P*,*P*)-**1** crown macrocycle at the CAM-B3LYP/6-31G(d) level of theory. For clarity, *tert*-butyl groups were replaced by methyl groups and hydrogens are not shown. Long arrows represent the linear motion of electrons in the butadiyne units, and short circular arrows give the rotational motion of electrons at the sp carbons of the allene units.

There is another mechanism to generate MTDM. In the HOMO (MO216), the p-orbital of the sp carbon in the

allene unit is directed to the *xy* plane, while in the LUMO (MO217), it is directed to the *z* axis (Scheme 2a). Therefore, due to the rotational motion (≈90°) of electrons at the sp carbon atoms of the allene units, this excitation generates local MTDMs, which are parallel to the allene axis. Since these four local MTDMs are circularly arranged, their *xy* components cancel each other, while the *z* component remains non-zero, due to the tilt of allenes into the *z* axis.

In a similar way, the features of transition S2 are qualitatively explained by the topology and symmetry of MOs (Figure 8b). Scheme 2b shows two representative MOs involved in the CIs of transition S2 together with the symmetrical character. The excitation from MO214 to MO217 generates four local ETDMs along the butadiyne units. By summing the four ETDM vectors, the *y* component vanishes because of the symmetry of MOs, while the ETDM vector is large in the *x* axis. Additionally, the *z* axis component also vanishes, because two ETDMs (1 and 2, see Scheme 2) are directed to the $+z$ axis, while the remaining two (3 and 4) are directed to the $-z$ axis (Figure 8b). The excitation transition MO214→MO217 is thus polarized in the plane of the ring (Figure 8b).

The ETDMs along the butadiyne axes also make non-zero MTDMs: the *z* axis components of two MTDMs generated by local ETDMs (1 and 3) cancel each other, while the *xy* components remain non-zero. The same is true for the MTDMs generated by ETDMs (2 and 4) and the *xy* components remain non-zero. The resulting MTDM is thus polarized in the *xy* plane (Figure 8b).

The local MTDMs (5 and 6) generated along the allene axis, also contribute to the MTDM. The *z* component vanishes, while the *x* component remains non-zero (Scheme 2b). Both ETDM and MTDM are thus polarized in the *xy* plane, which is consistent with the result shown in Figure 8b.

A similar qualitative analysis holds for the transition S3, because transitions S2 and S3 are degenerate. The explanation described before is thus helpful for understanding the mechanism of the intense chiroptical responses of this chiral macrocycle. In addition, it will allow the rational design of new shape-persistent alleno–acetylenic structures with optimal geometries, to maximize the chiroptical properties.

ELF analysis: During the analysis of the electronic structure of (*P*,*P*,*P*,*P*)-(−)-**1**, we found many π-like MOs with interesting topologies. Some of them are continuous tori, displaying many turns around the sigma frame. This interesting finding prompted us to investigate the nature of the aromaticity of this compound.

A common way to investigate aromaticity is through the nucleus-independent chemical shift (NICS), introduced by Schleyer and co-workers.[27] The original NICS(0) value (placed at the ring centroid) and further refinements, such as dissected $NICS_{zz}$[28] work well for systems in which a plane of symmetry can define the difference between σ and π symmetry, but they are less unique for nonplanar helical systems, in which only axes of symmetry can be formally defined. In addition, NICS values depend on the size of the ring and the distances from the centroid to the periphery, making comparison of our macrocycle with known systems difficult.

The ELF (electron localization function)[29] is an empirical function that has been used to indirectly study aromaticity in carbocycles,[7f,30] and nonplanar phyrins and annulenes.[19c,31] ELF has several advantages compared with ring-current derived methods. It does not require definition of a plane of symmetry with respect to an external applied magnetic field, it is not ring-size extensive, and it is nearly independent of the level of theory used to compute it. With these advantages, we decided to use ELF to explore the delocalization characteristics of the π-electron manifold in the macrocycle (*P*,*P*,*P*,*P*)-**1**.

ELF provides information about the delocalization of electrons. In the closed-shell density functional approach, the ELF function is related to the additional kinetic energy density of the electrons due to the Pauli principle. The function is normalized between the values of 0 and 1, with a value of 0.5 being that for a uniform electron gas of the same density. A volume of space enclosed by a particular ELF isosurface is termed a localization domain. These localization domains may be attractors (nuclei) or basins, with the latter representing core, valence, or non-bonding electrons. A common way to locate these basins is to inspect the ELF isosurface as it is increased from 0 to 1, and to identify the ELF values at which the continuous surface (at low thresholds) bifurcates into discrete basins associated with core, valence, or non-bonding electrons at higher thresholds. Thus, the valence basin for for example, a C−C bond typically bifurcates at ELF values of ≈0.95–0.99. The utility of ELF as a function for exploring aromaticity is derived from an ability to unambiguously partition the MOs into separate σ- and π-electron manifolds, a process that for molecules lacking a plane of symmetry can be based purely on the energy separation between the manifolds. When ELF is computed for the π-MOs only (denoted as ELF_π), the value of the function at which the valence π basins bifurcate can then be related to the aromatic or anti-aromatic π character. High bifurcation values correlate with clearly aromatic systems. Thus for benzene, the threshold is ≈0.9[32] (for a rotatable 3D model of the ELF_π function at this threshold, see the interactive version of Figure 9 in the HTML version of the article or in the Supporting Information). This property appears to be independent of the size of the annulene. Thus, [26]annulene appears to be the largest simply conjugated planar π carbocycle[26] that sustains a delocalized non-alternating geometry[33] and its ELF_π bifurcation value is ≈0.89, virtually the same as benzene (interactive version of Figure 9 in the HTML version of the article or in the Supporting Information). A crystal structure of a similarly sized and also highly nonplanar annulene[24] (with D_{2d} symmetry) has been reported.[34] This structure has a more prominently bond-alternating geometry, and this fact is also associated with a very much lower ELF_π bifurcation value of 0.135. This would be consistent with either anti-aromaticity or

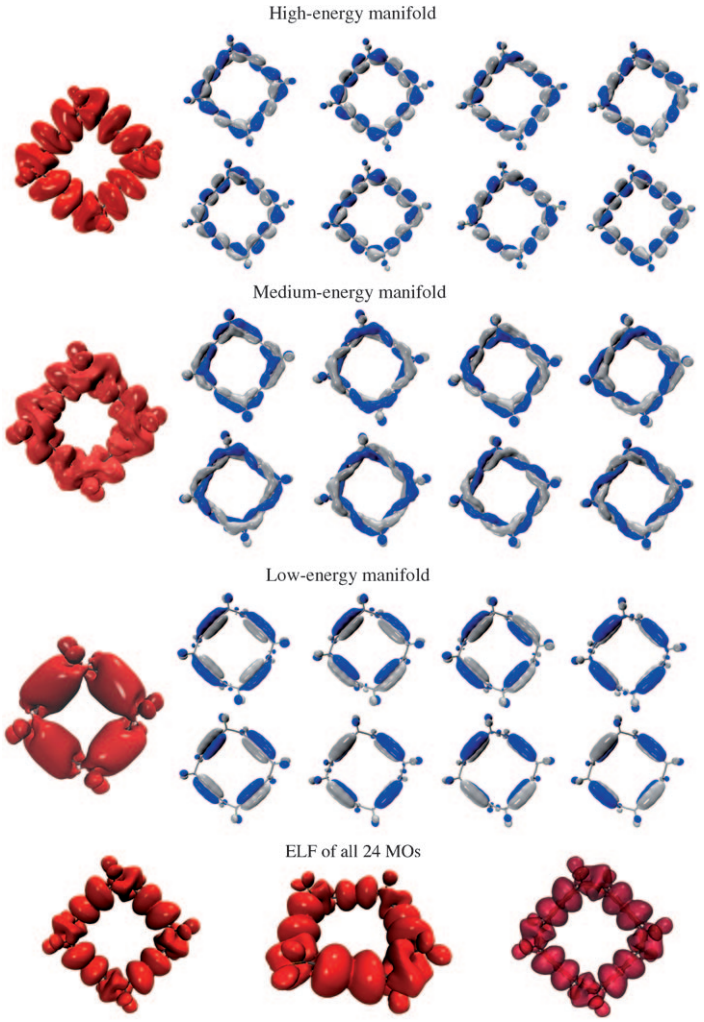

Figure 9. Canonical MOs (isovalue = 0.02, blue and white surfaces) and ELF_{π} (red surfaces) plotted at the bifurcation value (0.05). The lowest row shows different orientations (and a semitransparent representation, right) of the ELF_{π} surface of the combined manifolds (MOs 97–120) at the bifurcation value. 3D-rotatable structures of all surfaces can be found in the interactive version of Figure 9 at www.wiley-vch.de/contents/jc_2111/2010/chem.201001087/Figure9/ or in the Supporting Information.

non-aromaticity, as would be appropriate for a $4n$ rather than a $4n+2$ π-electron system. One final calibrant, which bears most similarity to **1** is the *carbo*-benzene **5** (Scheme 3), which has been shown to be an 18-π aromatic with a strongly diatropic circulation around the main ring.[30a] The ELF_{π} bifurcation threshold (B3LYP/6-31G*) for the main ring is ≈0.69, whilst that for the phenyl groups

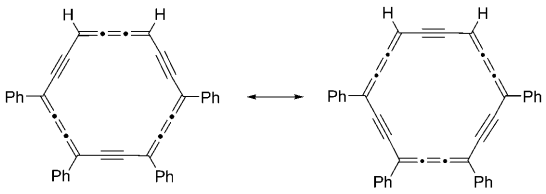

Scheme 3. Structure of **5**. Resonant structures proposed by Chauvin and co-workers.[30a]

is ≈0.79 (interactive version of Figure 9 in the HTML version of the article or in the Supporting Information).

In order to apply this technique to our systems, it is first necessary to identify pure π MOs. In the macrocycle (*P*,*P*,*P*,*P*)-(−)-**1** that was actually synthesized, this is not possible due to the mixing of σ orbitals of the *tert*-butyl substituents with the π manifold, evidently owing to the lack of planes of symmetry, but also to the lack of a clear energy separation between the two manifolds. To reduce this σ–π mixing, F atoms[19a] were used in the calculations to replace the *tert*-butyl substituents of the original structure. This increases the energy gap between the σ–π manifolds and results in essentially pure π MOs.

Our system is composed of 24 clearly identifiable π MOs. These can be classified into three submanifolds according to their energy and topology. The low-energy manifold encompasses MOs 97 to 104 (Figure 9). They share the common feature of being continuous in the butadiyne moiety and display a node around the sp carbon atoms of the allenes. The medium-energy manifold includes MOs 105 to 112 (Figure 9) and these MOs all have the topology of a torus link[35] with four, six, and eight half-turns around the σ framework. The high-energy manifold includes MOs 113 to 120 (MO 120 = HOMO, Figure 9). The lowest MOs of this manifold also display torus link topologies, with eight and ten half-turns, while the MOs closer to the HOMO show several nodes located at the single bonds connecting alkynes with allenes. The ELF_{π} surface derived from the combined 24 doubly-occupied π MOs has a bifurcation isovalue of 0.225, which clearly associates it with the characteristics of a non- or anti-aromatic annulene rather than that of a delocalized and aromatic system. Furthermore, this bifurcation occurs at the single bonds connecting allenes and alkynes, which were found experimentally (X-ray, see captions of Figure 3 and 4) to be the longest in the backbone. It is worth mentioning that there seems to be a relation between the energy of the MOs and their number of half-turns. Apparently, the number of half-turns (and not only the number of nodes) governs the energetic ordering of MOs. In order to identify the overall topology of the π system, one would need to inspect the form of the electron density $\rho(r)$ derived from π MO occupancy by either a total of 48 π electrons[35] or by three submanifolds of 16 electrons. Unfortunately, due the formation of many "wormholes" connecting torus link and torus knot topologies,[19c] this did not prove possible.

According to this analysis, macrocycles **1** belong to a relatively rare class of highly stable (even crystalline) non- or anti-aromatic molecules, of which a number of examples are known.[36] Since allenes impart a half-turn to π MOs, every cycle with an even number of allenes will be formally anti-aromatic, regardless of the chirality of the allene moieties. However, odd numbers of allenes could lead to Möbius aromatic compounds, which could display different chiroptical properties relative to their Hückel anti-aromatic counterparts. The synthesis and analysis of enantiopure alleno–acetylenic macrocycles bearing odd numbers of allenes is currently underway. Furthermore, future studies will also in-

clude analysis using the recently reported adaptive natural density partitioning method of Zubarev and Boldyrev,[37] which could bring new light to the investigation of the nature of aromaticity in nonplanar systems.

Conclusion

New alleno–acetylenic macrocycles have been prepared by oxidative homocoupling of optically active and racemic DEAs. The C_2-symmetric (*M*,*M*,*M*,*P*)-(+)-**1** and (*P*,*P*,*P*,*M*)-(−)-**1** enantiomers were obtained from optically enriched starting material, taking advantage of the statistical distribution of the stereoisomers, followed by separation of the diastereoisomers by HPLC techniques. The structures of all compounds were unambiguously assigned by full spectroscopic characterization, including X-ray crystallographic analyses of the chiral macrocycles.

Extensive computational studies showed that the new CAM-B3LYP hybrid functional correctly predicts the chiroptical properties of alleno–acetylenic macrocycles, consequently becoming the method of choice for future studies. The ab initio prediction of the vibronic structure observed in the UV/Vis and CD spectra of (*P*,*P*,*P*,*P*)-(−)-**1** proved to be extremely challenging. The main reason is the dense manifold of states around the transition of interest, which in combination with the high symmetry of the molecule might give rise to non-adiabatic effects.

Deeper understanding of the origin of the chiroptical response of alleno–acetylenic structures was obtained by analyzing the MOs involved in the main transitions. Furthermore, by examining the ELF_π function and the topology of the canonical MOs, we determined that the (*P*,*P*,*P*,*P*)-(−)-**1** isomer displays Hückel non- or anti-aromaticity. These studies provide a powerful tool for the design of molecular and supramolecular alleno–acetylenic structures with the potential to display unprecedented chiroptical responses. Current research in our group includes the synthesis and analysis of the chiroptical properties of smaller and larger macrocycles, as well as the functionalization of the side chains of DEAs to be used in various molecular and supramolecular applications.

Experimental Section

Materials and general methods: Reagents and solvents were purchased at reagent grade from Acros, Aldrich, and Fluka, and used as received. Toluene was purified by a solvent drying system from LC Technology Solutions Inc. SP-105 under nitrogen atmosphere (H_2O content <10 ppm as determined by Karl Fischer titration). THF was freshly distilled from sodium benzophenone ketyl under nitrogen atmosphere. Flash chromatography (FC) was carried out with SiO_2 60 (particle size 0.040–0.063 mm, 230–400 mesh; Fluka). Elution was done with distilled technical solvents. Thin-layer chromatography (TLC) was conducted on glass sheets coated with SiO_2 60 F_{254} obtained from Merck; visualization with a UV lamp (254 or 366 nm) and with a 10% solution of phosphomolybdic acid in ethanol. ^{1}H NMR and ^{13}C NMR spectra were measured at 25°C with a Varian Gemini 300, Bruker DRX 400, Bruker DRX 500, or a Bruker Avance III 600 spectrometer. Chemical shifts are reported in ppm relative to the signal of Me_4Si. Residual solvent signals in the ^{1}H and ^{13}C NMR spectra were used as an internal reference. Preparative recycling HPLC was run on a Japan Analytical Industry LC-9101 system with an L-7110 pump and a 3702 UV-detector. UV/Vis spectra were recorded on a Varian Cary-500 spectrophotometer. CD spectra were recorded on a Jasco J-715 spectropolarimeter. IR spectra were recorded on a Perkin–Elmer BX FT-IR spectrophotometer. The absorption wavelengths are reported in nm with the molar extinction coefficient ε ($M^{-1}cm^{-1}$) in brackets. HR-EI spectra were measured with a Waters Micromass AutoSpec-Ultima spectrometer and HR-FT-MALDI with an IonSpec Ultima Fourier transform (FT) instrument with 3-hydroxypicolinic acid (3-HPA) as matrix. The most important signals are reported in *m*/*z* units with $[M]^+$ as the molecular ion.

Computational methods: All optimizations, single-point energy, and excited states calculations were carried out using Gaussian 09.[38] For the ELF studies, the B3LYP functional was used with the 6–31G(d) basis set. ELF_π surfaces were calculated for the given set of (approximately) π MOs using Dgrid 4.5[39] and visualized with VMD[40] using the cube files obtained from Dgrid.

X-ray analysis: Both structures were solved by direct methods (SIR-97),[41] and refined by full-matrix least-squares analysis (SHELXL-97),[42] using an isotropic extinction correction. All non-hydrogen atoms were refined anisotropically; hydrogen atoms isotropically, whereby hydrogen atom positions are based on stereochemical considerations.

X-ray crystal structure of (*M*,*M*,*M*,*M*)/(*P*,*P*,*P*,*P*)-1: Crystal data at 260(2) K for $C_{60}H_{72}$, $M_r=793.18$, tetragonal, space group *P*4/*nnc* (no. 126), $\rho_{calcd}=0.765\ g\,cm^{-3}$, $Z=6$, $a=b=19.245(4)$, $c=27.881(6)$ Å, $V=10326(4)$ Å^3. Bruker-Nonius Kappa-CCD, $Mo_{K\alpha}$ radiation, $\lambda=0.7107$ Å, $\mu=0.043\ mm^{-1}$. A colorless, highly solvated, and fragile crystal of (*M*,*M*,*M*,*M*)/(*P*,*P*,*P*,*P*)-**1** (linear dimensions ca. $0.50\times0.30\times0.28$ mm) was obtained by slow evaporation of a mixture of hexane/ethanol/methanol 9:0.5:0.5. It was mounted at low temperature to prevent evaporation of enclosed solvents. The investigated crystals did not diffract to high θ and shatter below about 250 K. Numbers of measured and unique reflections are 38308 and 3115, respectively ($R_{int}=0.086$). There are two independent conformers (C_2- and D_4-symmetric), which are located in different special positions. Final $R(F)=0.123$, $wR(F^2)=0.320$ for 214 parameters and 2295 reflections with $I>2\sigma(I)$ and $1.50<\theta<21.97°$ (corresponding *R* values based on all 3115 reflections are 0.163 and 0.339, respectively). The final difference map contains 12 weak electron-density peaks between about 0.3 and 0.7 e Å^{-3}. They must be due to highly disordered solvents, which are located in the voids of the crystal lattice. When these weak peaks are included as carbon atoms (isotropic *U* values ca. 0.5 to 0.9 Å^2) in the structure factor calculation, $R(F)$ and $wR(F^2)$ based on 2295 reflections with $I>2\sigma(I)$ decrease to about 0.09 and 0.24, respectively, and ρ_{calcd} increases to 0.99 g cm^{-3}.

X-ray crystal structure of (*P*,*P*,*P*,*M*)/(*M*,*M*,*M*,*P*)-1: Crystal data at 220(2) K for $(C_{60}H_{72})_2{\cdot}CH_3OH{\cdot}2H_2O$, $M_r=1652.19$, monoclinic, space group $P2_1/n$ (no. 14), $\rho_{calcd}=0.951\ g\,cm^{-3}$, $Z=2$, $a=12.8969(12)$, $b=30.468(2)$, $c=15.3610(13)$ Å, $\beta=107.645(12)°$, $V=5752.0(9)$ Å^3. Bruker-Nonius Kappa-CCD, $Mo_{K\alpha}$ radiation, $\lambda=0.7107$ Å, $\mu=0.055\ mm^{-1}$. A colorless crystal of (*P*,*P*,*P*,*M*)/(*M*,*M*,*M*,*P*)-**1** (linear dimensions ca. $0.21\times0.15\times0.13$ mm) was obtained by slow evaporation of a mixture of hexane/ethanol/methanol 9:0.5:0.5. The crystal was mounted at low temperature to prevent evaporation of enclosed solvents. Numbers of measured and unique reflections are 18693 and 10373, respectively ($R_{int}=0.035$). The CH_3OH solvent is disordered. Final $R(F)=0.082$, $wR(F^2)=0.216$ for 601 parameters and 6994 reflections with $I>2\sigma(I)$ and $2.70<\theta<25.34°$ (corresponding *R* values based on all 10373 reflections are 0.119 and 0.245, respectively).

CCDC-773842 ((*P*,*P*,*P*,*M*)/(*M*,*M*,*M*,*P*)-**1**) and -773843 ((*M*,*M*,*M*,*M*)/(*P*,*P*,*P*,*P*)-**1**) contain the supplementary crystallographic data for this paper. These data can be obtained free of charge from The Cambridge Crystallographic Data Centre via www.ccdc.cam.ac.uk/data_request/cif.

Synthesis and HPLC separation: The synthesis of macrocycles **1** has been previously described, along with the properties of (*P*,*P*,*P*,*P*)-(−)-**1** and (*M*,*M*,*M*,*M*)-(+)-**1**.[9] The mixture of isomers of **1** was separated by recy-

cling HPLC, using a Merck Hibar® LiChroshper® Si 60 (5 μm) preparative (250–25 mm) stationary phase, eluting with *n*-hexane (Merck LiChrosolv®) at 9 mL min^{-1}. Isomer (*P*,*M*,*P*,*M*)-**1** showed the shortest retention time, and was collected after the second cycle. Racemate (*M*,*M*,*M*,*M*)/(*P*,*P*,*P*,*P*)-**1** shows the longer retention time and can be collected in the fifth or sixth cycle. Separation of the racemate (*M*,*M*,*M*,*P*)/(*P*,*P*,*P*,*M*)-**1** and isomer (*P*,*P*,*M*,*M*)-**1** was only possible after the tenth cycle. ^{13}C NMR spectra can be found in the Supporting Information.

(*M*,*M*,*M*,*P*)-1,3,8,10,15,17,22,24-Octa-*tert*-butylcyclooctacosa-1,2,8,9,15,16,22,23-octaen-4,6,11,13,18,20,25,27-octayne ((*M*,*M*,*M*,*P*)-(+)-1): M.p. > 185 °C (decomp); $[\alpha]_D^{20} = +536$, ($c = 0.01$ in *n*-hexane); ^{1}H NMR (400 MHz, $CDCl_3$) $\delta = 1.153$ (s, 18H, *t*Bu), 1.157 (s, 18H, *t*Bu), 1.161 (s, 18H, *t*Bu), 1.163 ppm (s, 18H, *t*Bu); ^{13}C NMR (100 MHz, $CDCl_3$) $\delta =$ 29.14, 29.16, 29.17 (2), 35.80, 35.81, 35.87, 35.92, 75.25, 75.40, 75.44, 75.45, 77.93, 77.96, 77.97 (2), 104.00 (2), 104.01, 104.06, 216.28, 216.54 (2), 216.78 ppm; IR (ATR): $\tilde{\nu} = 2964$ (s), 2930 (m), 2903 (m), 2867 (m) 2357 (vw), 2164 (vw), 1983 (vw), 1919 (vw), 1475 (m), 1459 (m), 1393 (w), 1363 (s), 1222 (m), 1077 (s), 1022 (w), 936 (w), 906 (w), 633 cm^{-1} (w); UV/Vis (*n*-hexane): λ_{max} (ε) = 323 (26700), 300 (51900), 281 (57800), 242 nm (212900); MALDI-MS: *m/z* (%): 832 (4) $[M+K]^+$, 816 (11) $[M+Na]^+$, 794 (100) $[M+H]^+$; HR-MALDI-MS: *m/z* calcd for $C_{60}H_{73}^+$: 793.5707; found: 793.5722 $[M+H]^+$. The enantiomer (*P*,*P*,*P*,*M*)-(+)-**1** was obtained similarly: $[\alpha]_D^{20} = -530$, ($c = 0.007$ in *n*-hexane).

(*P*,*P*,*M*,*M*)-1,3,8,10,15,17,22,24-Octa-*tert*-butylcyclooctacosa-1,2,8,9,15,16,22,23-octaen-4,6,11,13,18,20,25,27-octayne ((*P*,*P*,*M*,*M*)-1): M.p. > 230 °C (decomp); ^{1}H NMR (600 MHz, $CDCl_3$) $\delta = 1.153$ (s, 36H, *t*Bu), 1.165 ppm (s, 36H, *t*Bu); ^{13}C NMR (150 MHz, $CDCl_3$) $\delta = 28.98$, 29.00, 35.63, 35.76, 75.20, 75.33, 77.76, 77.82, 103.87, 103.89, 216.36 ppm; IR (ATR): $\tilde{\nu} = 2960$ (s), 2925 (s), 2866 (s), 2358 (vw), 2324 (vw), 2163 (vw), 1914 (w), 1737 (w), 1661 (w), 1636 (w), 1475 (s), 1460 (s), 1393 (m), 1362 (s), 1261 (m), 1244 (m), 1222 (m), 1024 (s), 906 cm^{-1} (s); UV/Vis (*n*-hexane): λ_{max} (ε) = 323 (30200), 300 (44000), 282 (44900), 242 nm (116600); MALDI-MS: *m/z* (%): 832 (5) $[M+K]^+$, 816 (18) $[M+Na]^+$, 794 (100) $[M+H]^+$; HR-MALDI-MS: *m/z* calcd for $C_{60}H_{73}^+$: 793.5707; found: 793.5715 $[M+H]^+$.

(*P*,*M*,*P*,*M*)-1,3,8,10,15,17,22,24-Octa-*tert*-butylcyclooctacosa-1,2,8,9,15,16,22,23-octaen-4,6,11,13,18,20,25,27-octayne ((*P*,*M*,*P*,*M*)-1): M.p. > 200 °C (decomp); ^{1}H NMR (500 MHz, $CDCl_3$) $\delta = 1.159$ ppm (s, 72H, *t*Bu); ^{13}C NMR (125 MHz, $CDCl_3$) $\delta = 29.14$, 35.84, 75.43, 78.00, 104.03, 216.42 ppm; IR (ATR): $\nu = 2961$ (s), 2926 (s), 2864 (m), 2210 (vw), 1983 (vw), 1912 (w), 1732 (w), 1476 (s, sh), 1458 (s), 1393 (m), 1362 (s), 1223 (m), 1209 (m, sh), 1080 (s), 1022 (w), 914 (w), 671 (w), 635 cm^{-1} (m); UV/Vis (*n*-hexane): λ_{max} (ε) = 322 (32300), 299 (50700), 281 (43800), 244 (128000), 233 nm (90000); MALDI-MS: *m/z* (%): 832 (4) $[M+K]^+$, 816 (15) $[M+Na]^+$, 794 (100) $[M+H]^+$; HR-MALDI-MS: *m/z* calcd for $C_{60}H_{73}^+$: 793.5707; found: 793.5718 $[M+H]^+$.

Acknowledgements

This work was supported by the ETH Research Council, a doctoral fellowship to P.R.-F. from the Stipendienfonds der Schweizerischen Chemischen Industrie (SSCI), and in part by the ERC Advanced Grant No. 246637 ("OPTELOMAC"). We acknowledge the C4 Competence Center for Computational Chemistry at ETH Zurich and CESGA (Santiago de Compostela, Spain) for the allocation of computational resources. N.B. and A.G.P. thank Columbia University research funds for financial support. Prof. K. Nakanishi is acknowledged for discussions and for sponsoring part of the stay of J.L.A.-G. at Columbia University. F.S. is grateful to CASPUR (project Standard Grant HPC 2009) and CNR-Village Network (http://village.ipcf.cnr.it) for computational resources.

[1] a) J. Zhang, J. S. Moore, *J. Am. Chem. Soc.* **1994**, *116*, 2655–2656; b) S. Höger, V. Enkelmann, K. Bonrad, C. Tschierske, *Angew. Chem.* **2000**, *112*, 2355–2358; *Angew. Chem. Int. Ed.* **2000**, *39*, 2267–2270; c) M. Fischer, G. Lieser, A. Rapp, I. Schnell, W. Mamadouh, S. de Feyter, F. C. de Schryver, S. Höger, *J. Am. Chem. Soc.* **2004**, *126*, 214–222; d) H. Shimura, M. Yoshio, T. Kato, *Org. Biomol. Chem.* **2009**, *7*, 3205–3207.

[2] a) A. S. Shetty, J. Zhang, J. S. Moore, *J. Am. Chem. Soc.* **1996**, *118*, 1019–1027; b) Y. Tobe, N. Utsumi, K. Kawabata, A. Nagano, K. Adachi, S. Araki, M. Sonoda, K. Hirose, K. Naemura, *J. Am. Chem. Soc.* **2002**, *124*, 5350–5364; c) Y. Saiki, K. Nakamura, Y. Nigorikawa, M. Yamaguchi, *Angew. Chem.* **2003**, *115*, 5348–5350; *Angew. Chem. Int. Ed.* **2003**, *42*, 5190–5192; d) S. Klyatskaya, N. Dingenouts, C. Rosenauer, B. Müller, S. Höger, *J. Am. Chem. Soc.* **2006**, *128*, 3150–3151.

[3] a) D. Venkataraman, S. Lee, J. Zhang, J. S. Moore, *Nature* **1994**, *371*, 591–593; b) D. L. Gin, W. Gu, *Adv. Mater.* **2001**, *13*, 1407–1410; c) S. Höger, D. L. Morrison, V. Enkelmann, *J. Am. Chem. Soc.* **2002**, *124*, 6734–6736; d) K. Kumeda, M. Ono, A. Kawai, H. Oike, K. Noguchi, N. Yonezawa, *Chem. Lett.* **2008**, *37*, 660–661; e) K. Raatikainen, J. Huuskonen, M. Lahtinen, P. Metrangolo, K. Rissanen, *Chem. Commun.* **2009**, 2160–2162.

[4] a) S. Höger, K. Bonrad, A. Mourran, U. Beginn, M. Möller, *J. Am. Chem. Soc.* **2001**, *123*, 5651–5659; b) S. Lei, A. Ver Heyen, S. De Feyter, M. Surin, R. Lazzaroni, S. Rosenfeldt, M. Ballauff, P. Lindner, D. Mössinger, S. Höger, *Chem. Eur. J.* **2009**, *15*, 2518–2535; c) D. Mössinger, D. Chaudhuri, T. Kudernac, S. Lei, S. De Feyter, J. M. Lupton, S. Höger, *J. Am. Chem. Soc.* **2010**, *132*, 1410–1423.

[5] For selected examples, see: a) S. Anderson, U. Neidlein, V. Gramlich, F. Diederich, *Angew. Chem.* **1995**, *107*, 1722–1725; *Angew. Chem. Int. Ed. Engl.* **1995**, *34*, 1596–1600; b) D. L. Morrison, S. Höger, *Chem. Commun.* **1996**, 2313–2314; c) Y. Tobe, N. Utsumi, A. Nagano, K. Naemura, *Angew. Chem.* **1998**, *110*, 1347–1349; *Angew. Chem. Int. Ed.* **1998**, *37*, 1285–1287; d) Y. Hosokawa, T. Kawase, M. Oda, *Chem. Commun.* **2001**, 1948–1949; e) T. Kawase, K. Tanaka, N. Shiono, Y. Seirai, M. Oda, *Angew. Chem.* **2004**, *116*, 1754–1756; *Angew. Chem. Int. Ed.* **2004**, *43*, 1722–1724.

[6] a) R. R. Tykwinski, U. Gubler, R. E. Martin, F. Diederich, C. Bosshard, P. Günter, *J. Phys. Chem. B* **1998**, *102*, 4451–4465; b) A. Sarkar, J. J. Pak, G. W. Rayfield, M. M. Haley, *J. Mater. Chem.* **2001**, *11*, 2943–2945; c) M. B. Nielsen, M. Schreiber, Y. G. Baek, P. Seiler, S. Lecomte, C. Boudon, R. R. Tykwinski, J.-P. Gisselbrecht, V. Gramlich, P. J. Skinner, C. Bosshard, P. Günter, M. Gross, F. Diederich, *Chem. Eur. J.* **2001**, *7*, 3263–3280; d) A. Bhaskar, R. Guda, M. M. Haley, T. Goodson III, *J. Am. Chem. Soc.* **2006**, *128*, 13972–13973.

[7] For selected examples, see: a) J. Anthony, C. B. Knobler, F. Diederich, *Angew. Chem.* **1993**, *105*, 437–440; *Angew. Chem. Int. Ed. Engl.* **1993**, *32*, 406–409; b) T. Nishinaga, T. Kawamura, K. Komatsu, *J. Org. Chem.* **1997**, *62*, 5354–5362; c) M. Schreiber, R. R. Tykwinksi, F. Diederich, R. Spreiter, U. Gubler, C. Bosshard, I. Poberaj, P. Günter, C. Boudon, J.-P. Gisselbrecht, M. Gross, U. Jonas, H. Ringsdorf, *Adv. Mater.* **1997**, *9*, 339–343; d) F. Diederich, L. Gobbi, *Top. Curr. Chem.* **1999**, *201*, 43–79; e) F. Mitzel, C. Boudon, J.-P. Gisselbrecht, M. Gross, P. Seiler, F. Diederich, *Chem. Commun.* **2002**, 2318–2319; f) C. Lepetit, M. B. Nielsen, F. Diederich, R. Chauvin, *Chem. Eur. J.* **2003**, *9*, 5056–5066; g) M. Kivala, F. Mitzel, C. Boudon, J.-P. Gisselbrecht, P. Seiler, M. Gross, F. Diederich, *Chem. Asian J.* **2006**, *1*, 479–489; h) G. Chen, I. Mahmud, L. N. Dawe, Y. Zhao, *Org. Lett.* **2010**, *12*, 704–707.

[8] a) L. Ma, L. Pu, *Macromol. Chem. Phys.* **1998**, *199*, 2395–2401; b) D. L. An, T. Nakano, A. Orita, J. Otera, *Angew. Chem.* **2002**, *114*, 179–181; *Angew. Chem. Int. Ed.* **2002**, *41*, 171–173; c) T. Ishikawa, T. Shimasaki, H. Akashi, S. Toyota, *Org. Lett.* **2008**, *10*, 417–420.

[9] J. L. Alonso-Gómez, P. Rivera-Fuentes, N. Harada, N. Berova, F. Diederich, *Angew. Chem.* **2009**, *121*, 5653–5656; *Angew. Chem. Int. Ed.* **2009**, *48*, 5545–5548.

[10] a) D. A. Plattner, Y. Li, K. N. Houk in *Modern Acetylene Chemistry* (Eds.: P. J. Stang, F. Diederich), Wiley-VCH, Weinheim, **1995**, pp. 1–32; b) R. Chauvin, C. Lepetit in *Acetylene Chemistry: Chemistry, Biology and Material Science* (Eds.: F. Diederich, P. J. Stang, R. R. Tykwinski), Wiley-VCH, Weinheim, **2005**, pp. 1–50.

[11] a) C. S. Jones, M. J. O'Connor, M. M. Haley in *Acetylene Chemistry: Chemistry, Biology and Material Science* (Eds.: F. Diederich, P. J. Stang, R. R. Tykwinski), Wiley-VCH, Weinheim, **2005**, pp. 303–385; b) W. Zhang, J. S. Moore, *Angew. Chem.* **2006**, *118*, 4524–4548; *Angew. Chem. Int. Ed.* **2006**, *45*, 4416–4439.

[12] a) C. Grave, A. D. Schlüter, *Eur. J. Org. Chem.* **2002**, 3075–3098; b) Y. Yamaguchi, Z. Yoshida, *Chem. Eur. J.* **2003**, *9*, 5430–5440; c) U. H. F. Bunz, *J. Organomet. Chem.* **2003**, *683*, 269–287.

[13] F. Diederich, M. Kivala, *Adv. Mater.* **2010**, *22*, 803–812.

[14] a) V. Maraval, R. Chauvin, *Chem. Rev.* **2006**, *106*, 5317–5343; b) J. Sakamoto, J. van Heijst, O. Lukin, A. D. Schlüter, *Angew. Chem.* **2009**, *121*, 1048–1089; *Angew. Chem. Int. Ed.* **2009**, *48*, 1030–1069.

[15] P. Manini, W. Amrein, V. Gramlich, F. Diederich, *Angew. Chem.* **2002**, *114*, 4515–4519; *Angew. Chem. Int. Ed.* **2002**, *41*, 4339–4343.

[16] a) S. Odermatt, J. L. Alonso-Gómez, P. Seiler, M. M. Cid, F. Diederich, *Angew. Chem.* **2005**, *117*, 5203–5207; *Angew. Chem. Int. Ed.* **2005**, *44*, 5074–5078.

[17] P. Rivera-Fuentes, J. L. Alonso-Gomez, A. G. Petrovic, F. Santoro, N. Harada, N. Berova, F. Diederich, *Angew. Chem.* **2010**, *122*, 2296–2300; *Angew. Chem. Int. Ed.* **2010**, *49*, 2247–2250.

[18] For allenic and alleno–acetylenic cyclophane-type macrocycles, see: a) S. Thorand, F. Vögtle, N. Krause, *Angew. Chem.* **1999**, *111*, 3929–3931; *Angew. Chem. Int. Ed.* **1999**, *38*, 3721–3723; b) M. D. Clay, A. G. Fallis, *Angew. Chem.* **2005**, *117*, 4107–4110; *Angew. Chem. Int. Ed.* **2005**, *44*, 4039–4042; c) ref. [15]; d) M. Leclère, A. Fallis, *Angew. Chem.* **2008**, *120*, 578–582; *Angew. Chem. Int. Ed.* **2008**, *47*, 568–572; e) J. L. Alonso-Gomez, A. Navarro-Vazquez, M. M. Cid, *Chem. Eur. J.* **2009**, *15*, 6495–6503.

[19] a) S. Martin-Santamaría, H. S. Rzepa, *J. Chem. Soc. Perkin Trans. 2* **2000**, 2372–2377; b) S. Martin-Santamaría, B. Lavan, H. S. Rzepa, *Chem. Commun.* **2000**, 1089–1090; c) H. S. Rzepa, *Phys. Chem. Chem. Phys.* **2009**, *11*, 1340–1345.

[20] H. S. Rzepa, *Org. Lett.* **2009**, *11*, 3088–3091.

[21] J. L. Alonso-Gómez, P. Schanen, P. Rivera-Fuentes, P. Seiler, F. Diederich, *Chem. Eur. J.* **2008**, *14*, 10564–10568.

[22] R. Rossi, A. Carpita, C. Bigelli, *Tetrahedron Lett.* **1985**, *26*, 523–526.

[23] For a discussion, see: a) Z.-L. Cai, K. Sendt, J. R. Reimers, *J. Chem. Phys.* **2002**, *117*, 5543–5549; b) S. Grimme, M. Parac, *ChemPhysChem* **2003**, *4*, 292–295.

[24] T. Yanai, D. P. Tew, N. C. Nicholas, *Chem. Phys. Lett.* **2004**, *393*, 51–57.

[25] For selected examples, see: a) M. J. G. Peach, E. I. Tellgren, P. Salek, T. Helgaker, D. J. Tozer, *J. Phys. Chem. A* **2007**, *111*, 11930–11935; b) P. A. Limacher, K. V. Mikkelsen, H. P. Lüthi, *J. Chem. Phys.* **2009**, *130*, 194114/1–194114/7; c) D. Jacquemin, V. Wathelet, E. A. Perpete, C. Adamo, *J. Chem. Theory Comput.* **2009**, *5*, 2420–2435; d) J. Zhang, X. Guo, Z. Cao, *J. Chem. Phys.* **2009**, *131*, 144307/1–7; e) S. Borini, P. A. Limacher, H. P. Lüthi, *J. Phys. Chem. A* **2010**, *114*, 2221–2229.

[26] a) F. Santoro, R. Improta, A. Lami, J. Bloino, V. Barone, *J. Chem. Phys.* **2007**, *126*, 084509/1–084509/13; b) H. Köppel in *Conical Intersections, Electronic Structure, Dynamics and Spectroscopy* (Eds.: W. Domcke, D. R. Yarkony, H. Köppel), World Scientific Publishing, Singapore, **2004**, pp. 429–472; c) for further details, see the Supporting Information.

[27] P. von R. Schleyer, C. Maerker, A. Dransfeld, H. Jiao, N. J. R. v. E. Hommes, *J. Am. Chem. Soc.* **1996**, *118*, 6317–6318.

[28] For a review, see: Z. Chen, C. S. Wannere, C. Corminboeuf, R. Puchta, P. von R. Schleyer, *Chem. Rev.* **2005**, *105*, 3842–3888.

[29] a) A. D. Becke, K. E. Edgecombe, *J. Chem. Phys.* **1990**, *92*, 5379–5403; b) B. Silvi, A. Savin, *Nature* **1994**, *371*, 683–686.

[30] a) C. Saccavini, C. Sui-Seng, L. Maurette, C. Lepetit, S. Soula, C. Zou, B. Donnadieu, R. Chauvin, *Chem. Eur. J.* **2007**, *13*, 4914–4931; b) A. Soncini, P. W. Fowler, C. Lepetit, R. Chauvin, *Phys. Chem. Chem. Phys.* **2008**, *10*, 957–964; c) M. Gicquel, J.-L. Heully, C. Lepetit, R. Chauvin, *Phys. Chem. Chem. Phys.* **2008**, *10*, 3578–3589.

[31] a) C. S. M. Allan, H. S. Rzepa, *J. Org. Chem.* **2008**, *73*, 6615–6622; b) C. S. M. Allan, H. S. Rzepa, *J. Chem. Theory Comput.* **2008**, *4*, 1841–1848; c) C. S. Wannere, H. S. Rzepa, B. C. Rinderspacher, A. Paul, C. S. M. Allan, H. F. Schaefer III, P. von R. Schleyer, *J. Phys. Chem. A* **2009**, *113*, 11619–11629.

[32] J. C. Santos, W. Tiznado, R. Contreras, P. Fuentealba, *J. Chem. Phys.* **2004**, *120*, 1670–1673.

[33] a) S. S. Shaik, P. C. Hiberty, *A Chemist's Guide to Valence Bond Theory*, Wiley, New York, **2007**; b) H. S. Rzepa, Abstracts of Papers, 237th ACS National Meeting, Salt Lake City, UT, USA, March 22–26, **2009**, COMP-200.

[34] G. Wilke, *Angew. Chem.* **1988**, *100*, 189–211; *Angew. Chem. Int. Ed. Eng.* **1988**, *27*, 185–206.

[35] S. M. Rappaport, H. S. Rzepa, *J. Am. Chem. Soc.* **2008**, *130*, 7613–7619.

[36] For some recent examples of organic molecules, see: a) Q. Miao, T.-Q Nguyen, T. Someya, G. B. Blanchet, C. Nuckolls, *J. Am. Chem. Soc.* **2003**, *125*, 10284–10287; b) S. Miao, P. von R. Schleyer, J. I. Wu, K. I. Hardcastle, U. H. F. Bunz, *Org. Lett.* **2007**, *9*, 1073–1076; c) S. Miao, S. M. Brombosz, P. von R. Schleyer, J. I. Wu, S. Barlow, S. R. Marder, K. I. Hardcastle, U. H. F. Bunz, *J. Am. Chem. Soc.* **2008**, *130*, 7339–7344; d) J. I. Wu, C. S. Wannere, Y. Mo, P. von R. Schleyer, U. H. F. Bunz, *J. Org. Chem.* **2009**, *74*, 4343–4349.

[37] D. Y. Zubarev, A. I. Boldyrev, *Phys. Chem. Chem. Phys.* **2008**, *10*, 5207–5217.

[38] Gaussian 09, Revision A.02, M. J. Frisch, G. W. Trucks, H. B. Schlegel, G. E. Scuseria, M. A. Robb, J. R. Cheeseman, G. Scalmani, V. Barone, B. Mennucci, G. A. Petersson, H. Nakatsuji, M. Caricato, X. Li, H. P. Hratchian, A. F. Izmaylov, J. Bloino, G. Zheng, J. L. Sonnenberg, M. Hada, M. Ehara, K. Toyota, R. Fukuda, J. Hasegawa, M. Ishida, T. Nakajima, Y. Honda, O. Kitao, H. Nakai, T. Vreven, J. A. Montgomery, Jr., J. E. Peralta, F. Ogliaro, M. Bearpark, J. J. Heyd, E. Brothers, K. N. Kudin, V. N. Staroverov, R. Kobayashi, J. Normand, K. Raghavachari, A. Rendell, J. C. Burant, S. S. Iyengar, J. Tomasi, M. Cossi, N. Rega, J. M. Millam, M. Klene, J. E. Knox, J. B. Cross, V. Bakken, C. Adamo, J. Jaramillo, R. Gomperts, R. E. Stratmann, O. Yazyev, A. J. Austin, R. Cammi, C. Pomelli, J. W. Ochterski, R. L. Martin, K. Morokuma, V. G. Zakrzewski, G. A. Voth, P. Salvador, J. J. Dannenberg, S. Dapprich, A. D. Daniels, O. Farkas, J. B. Foresman, J. V. Ortiz, J. Cioslowski, D. J. Fox, Gaussian, Inc., Wallingford CT, **2009**.

[39] DGrid, version 4.5, M. Kohout, Radebeul, **2009**.

[40] W. Humphrey, A. Dalke, K. Schulten, *J. Mol. Graphics* **1996**, *14*, 33–38.

[41] A. Altomare, M. C. Burla, M. Camalli, G. L. Cascarano, C. Giacovazzo, A. Guagliardi, A. G. G. Moliterni, G. Polidori, R. Spagna, *J. Appl. Crystallogr.* **1999**, *32*, 115–119.

[42] SHELXL-97, Program for the Refinement of Crystal Structures, G. M. Sheldrick, University of Göttingen (Germany), **1997**.

Received: April 23, 2010
Published online: August 2, 2010

